Materials and Structures (2022) 55:176
https://doi.org/10.1617/s11527-022-02011-w

ORIGINAL ARTICLE

Direction-dependent behaviour and size effect of steel fibre reinforced concrete based on the double punch test

Simon Karrer · Tomislav Markić · Minu Lee · Jaime Mata-Falcón · Ali Amin · Walter Kaufmann

Received: 23 March 2022 / Accepted: 14 July 2022 / Published online: 6 August 2022

Abstract The post-cracking behaviour of steel fibre reinforced concrete (SFRC) is typically determined following an inverse analysis of flexural prism tests. Although these tests have significant practical merit, it has been argued that the anisotropy of the material due to the dispersion and orientation of the fibres cannot be accounted for in these tests. Multidirectional double punch tests on cubes have been proposed to overcome these issues. These tests are also well-suited to study size effects. However, no generally accepted inverse analysis method for these tests presently exists. This paper presents a simple and mechanically consistent inverse analysis procedure to estimate the residual post-cracking strength of SFRC from the results of double punch tests conducted on cubes. To explore the potential and limitations of this methodology, an experimental investigation was conducted on 30 double punch tests on cubes of varying sizes, varying fibre dosage and loading direction with respect to the concrete casting direction. The results demonstrate that the approach provides useful comparative information on the anisotropy of the material, however further investigation on the input parameters is required to prove its reliability in quantifying the residual tensile stress offered by the fibres.

Keywords Steel fibre reinforced concrete · Size effect · Multidirectional test · Double punch test · Crack kinematics · Inverse analysis · Post-cracking characterisation · Fibre orientation

1 Introduction

The addition of fibres to concrete can significantly increase the toughness or post-cracking energy absorption properties of the otherwise brittle concrete [1–3]. The limited uptake of steel fibre reinforced concrete (SFRC) in industry practice can be attributed to the difficulty in establishing and accurately quantifying the behaviour of the material to a degree that is required to be easily incorporated into existing and new design procedures. The fundamental property when considering the design of a structural member composed of SFRC is its post-cracking residual tensile strength. This property is commonly described in terms of its stress vs crack width (σ-w) response.

Several well-accepted test methods have been proposed in the literature to characterise and establish the σ-w relationship of SFRC at the material level. The primary purpose of laboratory material testing is to

S. Karrer (✉) · T. Markić · M. Lee · J. Mata-Falcón · W. Kaufmann
Institute of Structural Engineering (IBK), ETH Zürich, Zurich, Switzerland
e-mail: karrer@ibk.baug.ethz.ch

A. Amin
School of Civil Engineering, The University of Sydney, Sydney, Australia

provide useful data from which material properties, as required for the design of structural elements made of the material, can be accurately established. In general terms, these methods for SFRC can be split into two categories, namely direct and indirect methods.

Direct methods include uniaxial tension tests. These tests are, in principle, the ideal (theoretical) tests that should be used to determine the σ-*w* relationship of SFRC [4–8]. The results obtained from these tests do not require an inverse analysis and can be directly processed into design models. There are, however, drawbacks of conducting direct tension tests on SFRC. These include the effect of the boundary conditions and the requirements for specialised equipment [9–12].

Indirect methods include prism bending and round determinate panel tests. These tests are relatively easy to manufacture and perform. The load-deformation response obtained from these tests must, however, be combined with an inverse analysis to establish the σ-*w* relationship. Indeed, several formulations have been developed and proposed in national codes of practice [13–15].

Although it is well established in the literature that the dispersion and orientation of fibres in SFRC can display some bias in directionality due to several factors such as the flow of concrete and vibration during casting [16–18], available inverse analysis procedures rarely take this into regard in an adequate manner [19]. An attempt to overcome this limitation may be to test specimens cut out in different directions from a larger specimen. However, this procedure is too expensive in time and labour to be conducted in routine material testing.

Chen proposed the double punch test on concrete cylinders in 1970 [20]. This test was an alternative to the split cylinder test (also known as the Brazilian test) in determining the tensile strength of plain concrete. This test consists of placing a short concrete cylinder, with equal height and diameter, vertically between the loading plates of a testing machine. The specimen is compressed by two steel punches which are placed centrally on the top and bottom surfaces of the specimen. The testing arrangement is attractive in that the tests are easy to perform and failure of the specimen is not confined to a predefined plane. Marti [21] highlighted that these tests are subject to a relatively low amount of scatter.

Molins et al. [22] proposed the double punch test on short cylinders for obtaining the σ-*w* relationship of SFRC. The authors have subsequently demonstrated that these tests can be a potential alternative to flexural prism tests [23–26]. The authors have also developed a constitutive model for FRC based on that test [27]. However, double punch tests on cylinders and prism bending tests share the same key limitation: they do not permit a practical investigation of the anisotropy of SFRC which can be induced by the potentially non-uniform distribution of the fibres and, more importantly, the orientation of the fibres within the concrete. Pujadas et al. [24] introduced the multidirectional double punch test on SFRC cubic specimens to try and overcome this drawback. These tests are again relatively easy to conduct and can also account for any bias in the directionality of the fibres by testing the cubes in different orientations with respect to the casting direction. Moreover, the simple specimen geometry is particularly suitable for more extensive test campaigns on specimens of different sizes, as is required for studying the size effect. Some preliminary results on the size effect for the cracking load of plain concrete and SFRC cubes have been previously reported by the authors of this paper [28]. A major limitation of multidirectional double punch tests on cubic SFRC specimens to date is the lack of a generally accepted inverse analysis procedure to establish the σ-*w* relationship of the material.

To this end, this paper presents a simple and mechanically consistent inverse analysis procedure to characterise the post-cracking behaviour of SFRC by means of a notional stress-crack width relationship from the results of multidirectional double punch tests. A detailed assessment of the crack kinematics is performed on all faces of the cube using optical measurement methods during testing and forms the basis of the proposed inverse analysis procedure. Furthermore, the results of a experimental campaign intending to investigate the post-cracking behaviour along with the anisotropy and size effect of SFRC cubes is also presented.

2 Experimental campaign

2.1 Specimens, materials and casting

Details of the experimental campaign are reported in [28] and a summary is presented herein. A total of 30 cubes of varying sizes (as summarised in Table 1)

Table 1 Properties of the double punch specimens

{fibre dosage} [kg/m^3]			{size} [mm]	{loading direction}
00	40	80	150	H
00	40	80	150	V
00	40	80	212	H
00	40	80	212	V
00	40	80	300	H
00	40	80	300	V
00	40	80	424	H
00	40	80	424	V
00	40	80	600	H
00	40	80	600	V

were manufactured and tested to failure. A C25/30 concrete with a maximum aggregate size of D_{max}= 16 mm was adopted in all tests. The SFRC specimens contained Dramix 3D 65/35 steel fibres, which were 0.55 mm in diameter, 35 mm long and had an ultimate notional tensile strength of 1350 MPa. The cubes differed in *fibre dosage*, *size*, and *loading direction,* and are designated using the following nomenclature: F{*fibre dosage*}-{*size*}-{*loading direction*}. Three fibre volumetric dosages were adopted, i.e., $\rho_f = 0$, 40 and 80 kg/m^3, which corresponds to 0, 0.5 and 1.0% by vol., respectively. The *size* of the cubes is characterised by the cubes side length, s = {150, 212, 300, 424, 600}; the smallest and largest specimens thus differed by a factor of four in terms of side length (relevant for the size effect), 16 in terms of cross-section (relevant for test machine capacity), and 64 in terms of volume (relevant for production). The *loading direction* {H, V} distinguishes between cubes that were loaded horizontally (H) or vertically (V) with respect to the casting direction, i.e., the applied load was either perpendicular (H) or parallel (V) to the direction of casting. An overview of the test specimens investigated is presented in Table 1 and Fig. 1. While the original campaign consisted of additional samples of smaller sizes (75 and 106 mm), these tests are not discussed herein because the results were found to be non-representative due to the fibres being excessively large relative to the specimen size [28]. Four prisms with dimensions of 150 mm × 150 mm × 550 mm were cast together with the double punch samples for the batches containing fibres and were tested to [13].

The concrete was sourced from a local Swiss ready-mix supplier and delivered by a typical concrete mixer truck. The same concrete was used to cast all three concrete mixtures (defined by their fibre dosage), with the intention of removing any inconsistencies caused by concrete mixing and supply. The initial mass of concrete contained in the truck-mounted agitator bowl was determined by the supplier by weighing the truck before and after loading it with the concrete constituents. At concrete delivery, the specific density of the fresh concrete was determined; this allowed a more precise estimation of the fresh concrete volume and the required amounts of fibres to be added. Additionally, a flow table test was performed to determine the workability of the concrete (500, 520 and 370 mm for batches with fibre dosages 0, 40 and 80 kg/m^3, respectively). The plain concrete specimens (*fibre dosage* = 0 kg/m^3) were cast first by measuring out a defined mass of concrete in a kibble so that a known mass of concrete remained in the agitator. Steel fibres were then gradually added to the agitator to produce a mix with a fibre dosage of 40 kg/m^3. Furthermore, some superplasticiser was added to the agitator to ensure a similar concrete consistency to the plain concrete mix and to minimise the vibration required during casting. The fibres and concrete were thoroughly mixed within the agitator for approximately 10 min. After satisfying quality controls of uniformity and workability, the 40 kg/m^3 specimens were cast. The procedure was repeated analogously to batch and cast the SFRC mix containing 80 kg/m^3 of fibres.

All specimens were cast in lubricated timber formwork. The three largest sets of the plain concrete cubes (s = 300, 424, and 600 mm), were vibrated with an immersed vibration needle. All other specimens were compacted on a vibrating table, using additional external vibrators for the s = 300, 424, and 600 mm SFRC specimens to ensure a uniform degree of compaction amongst all specimens. Care was taken to avoid over-compaction, which would otherwise lead to a non-uniform distribution of the fibres through the height of the specimens. After hardening, the casting surface of all specimens were ground to ensure coplanar, level surfaces for load introduction.

The specimens were tested in ascending order with respect to their size. Testing began at an age of 20 days and took place over a period of 7 days. The

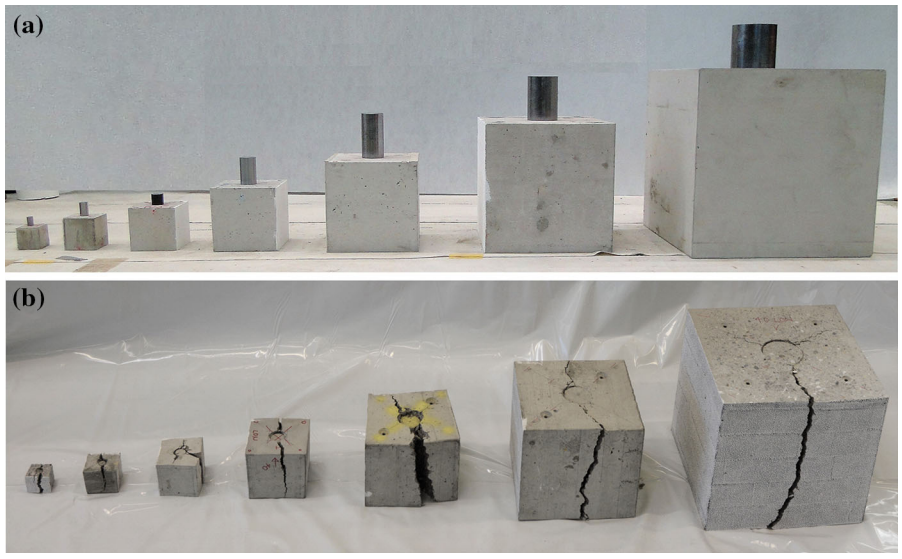

Fig. 1 Double punch specimens with *size* = {150, 212, 300, 424, 600} mm and *fibre dosage* = 40 kg/m^3: **a** before and **b** after testing

mechanical properties of the concrete (cylinder compressive strength f_c, modulus of elasticity E_c and tensile strength f_{ct}) and the flexural residual tensile strength offered by the SFRC (f_{Ri}) were determined 24 days after casting. These results are summarised in Table 2. The tensile strength was obtained by means of conventional cylindrical double punch tests as proposed by Chen [20]:

$$f_{ct} = \frac{4 \cdot N_{cr}}{\pi(2.4Dh - p^2)} \quad (1)$$

where N_{cr} is the cracking load of the specimen, D = 150 mm and h = 150 mm correspond to the cylinder diameter and height, respectively, and $p = D/4$ is the punch diameter.

2.2 Test protocol and instrumentation

As proposed by Chen [20], the diameter p of the steel punches used in this study was one-quarter of the side length s of the cube (see Fig. 2), i.e., p was scaled in proportion to s similar to the size-effect tests on plain concrete cubes conducted by Marti [21]. The punches were carefully centred on the loading surfaces to minimise any induced eccentricities. During the test, the ram displacement and the force signal of the machine were recorded. The test was terminated at a loss of approximately 80% of the peak load or at a maximum ram displacement of 15 mm, whichever occurred first.

The deformation of the cubes was tracked throughout testing using two measurement systems (see Fig. 3) on adjacent sides of each cube: (i) optical 3D motion tracking system 'Optotrak Certus' from NDI [29] (referred in the following as NDI) and (ii) 3D digital image correlation (DIC) from Correlated Solutions [30]. On two adjacent side faces of the cube, horizontally aligned pairs of optical NDI markers were attached to the specimens. The number of pairs depended on the size of the specimens,

Table 2 Mechanical properties of the concrete mixes (mean value and coefficient of variation in brackets)

{*fibre dosage*} [kg/m3]	f_c [mm]	E_c [GPa]	f_{ct} [MPa]	f_{R1} [MPa]	f_{R2} [MPa]	f_{R3} [MPa]	f_{R4} [MPa]
00	38.6 (± 1.8%)	32.8 (± 3.4%)	3.24 (± 1.5%)	–	–	–	–
40	39.2 (± 1.5%)	31.6 (± 2.5%)	3.19 (± 3.1%)	5.05 (± 20.2%)	5.31 (± 20.3%)	4.75 (± 14.5%)	4.29 (± 15.4%)
80	43.9 (± 1.4%)	32.5 (± 0.9%)	3.64 (± 3.0%)	6.17 (± 18.0%)	6.30 (± 14.8%)	6.07 (± 15.5%)	5.91 (± 15.1%)

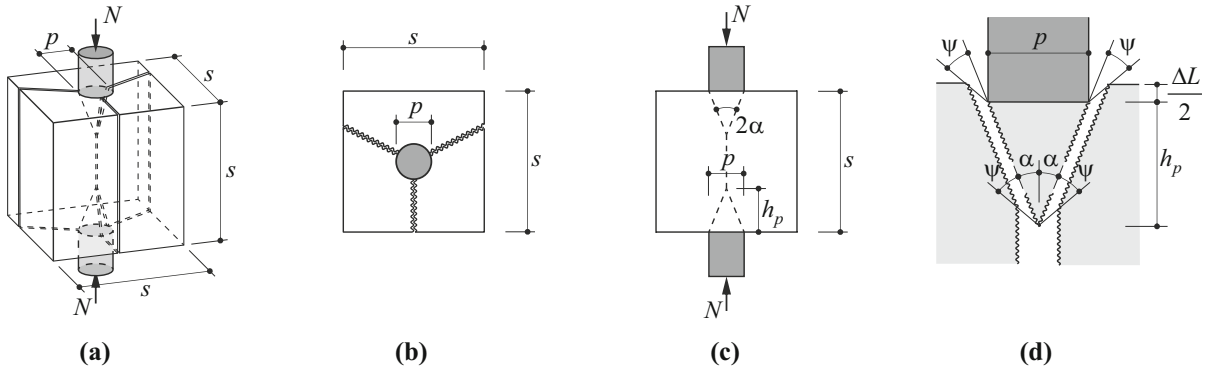

Fig. 2 Principle of multidirectional double punch test and typical failure mode assuming three cracks: **a** Isometric view with geometry; **b** plan view; **c** elevation view; **d** cone kinematics

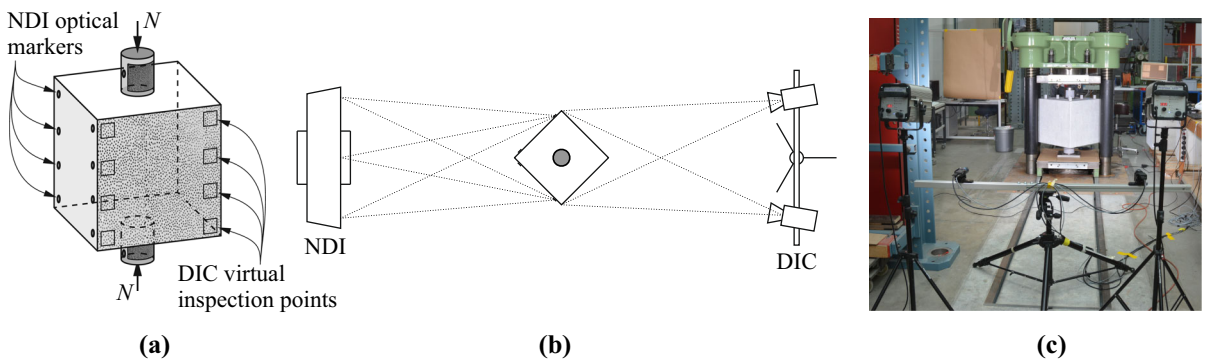

Fig. 3 Description of optical measuring systems: **a** Isometric view with the position of the optical markers and the speckle pattern; **b** plan view; **c** position of the DIC system for specimen with *size* = 600 mm

ranging from 3 equally spaced pairs for the smallest sized specimens to 7 equally spaced pairs for the largest specimens. On the other two adjacent side faces of the cube, a speckle pattern with a nominal speckle size of 2 mm was applied and tracked by DIC. Noting that the ram displacement measured by the testing machine is biased by the machine stiffness, NDI and DIC trackers were applied to the punches to compute the effective punch penetration into the concrete.

The extent of cracking of the specimens was continuously measured using these two measuring systems, both with a measurement frequency of 1 Hz. For the NDI system, 3-dimensional measurements were recorded. The crack widths along the specimen height were computed by determining the relative horizontal displacement between the pairs of optical markers. For the DIC measurements, a pair of high-resolution cameras (4096 × 3000 px and lenses with a focal length of 25 mm) were used to capture the images. During post-processing, the correlation was conducted using the software 'VIC-3D' by Correlated Solutions [30]. The crack widths were similarly extracted using the NDI system by computing the relative horizontal displacement of the DIC virtual inspection points placed in the same configuration as the NDI optical markers. The average value of the 3 to 7 crack width measurements by the NDI or DIC system represents the average crack width of that side of the cube. Using several pairs of inspection points allows cracks that do not open uniformly along the height of the cube to be adequately represented by the average crack width parameter. Finally, by summing up the average crack widths of the four sides of a particular cube, the *total perimetral crack width* (*TPCW*) is obtained as a representative proxy for the cracking behaviour of the cube. The threshold to consider a side of the cube as cracked was set to 0.1 mm, i.e., slightly above the uncertainty level of the NDI system. Average crack widths below this

threshold are not accounted toward the *TPCW*. In the following, only the *TPCW* will be focused on.

Setting the crack width equal to the relative horizontal displacement between pair of points located relatively far away from the crack is an approximation, as the relative horizontal displacement includes the small elastic deformation adjacent to the cracks. The accuracy of this approximation was examined by investigating the full displacement and strain fields of the surfaces tracked with DIC. Using the open-source software ACDM [31, 32], the cracks were detected, and the crack width was continuously computed based on the displacement and strain fields. The ACDM software allows multiple cracks to be detected and provides a much more precise measurement of the crack width since the inspection points are much closer to the crack. ACDM was applied to some randomly selected specimens, and the results demonstrated that the obtained crack width matched very closely to those obtained with the approximate crack width with simple virtual strain gauges [33]. Therefore, for the purpose of this paper, the discrete measurements of the crack width were judged to be sufficiently accurate.

3 Experimental results

3.1 General behaviour

When a concentrated load is applied over a limited area of concrete, the compressive stresses disperse below the loading plates, and circumferential tensile stresses develop within the specimen. These stresses are proportional to the applied load until the tensile strength of the concrete is reached and cracking occurs. For the specimens tested in this study, at cracking, a conical fragment develops adjacent to each steel punch, and vertical cracks propagate radially from these fragments across the width of the specimen. As the conical fragments penetrate the concrete with increasing ram displacements, the outer concrete segments are displaced in the radial direction. While a sliding failure occurs along the surface of the conical fragments, separation failure between the outer segments dominates the overall response of the specimens [20].

For most of the plain concrete specimens tested, three vertical cracks formed on the sides of the cubes, as shown in Figs. 2b and 4a. Although in several of the SFRC cubes three main radial cracks developed, many specimens displayed only two cracks (refer to Fig. 4b). Some SFRC specimens had cracks that opened relatively unevenly across the height of the cube.

With increasing penetration of the punches, the *TPCW* in the SFRC specimens tended to localise in the weakest radial crack plane. This is evident in Fig. 4b and 4c where the number of localised cracks in the specimens containing fibres was typically one. For the plain concrete specimens, the localisation of cracks cannot be observed because of the brittle nature of the material at the onset of cracking.

3.2 Wedge angle

After testing, the conical concrete fragments directly adjacent to the punches were extracted from the cubes. The effective geometry of the formed fragments was observed to be rather a 3- or 4-sided pyramid-like figure with a circular base as opposed to a perfect cone. The roughness of the crack surfaces also influences the effective geometry of the lateral surface of the fragments.

In order to simplify the proposed kinematic model, the fragments are assumed to be perfect cones. The angle of the cone α is defined in Fig. 2d, where h_p is the height of the cone and p the diameter of the punch:

$$\cot(\alpha) = \frac{2 \cdot h_p}{p} \tag{2}$$

Table 3 presents the observed value of $\cot(\alpha)$ for all specimens. Irrespective of *fibre dosage*, *size* and *loading direction*, the measured values of cot (α) did not exhibit significant variation among all specimens. The mean value of $\cot(\alpha)$ for all specimens tested was 2.14 (with a coefficient of variation (CoV) of 0.14). This corresponds to a cone angle of α = 25 deg. This is in perfect agreement with Pujadas' findings on double punch tests on FRC cylinders [23].

3.3 Fibre distribution

Aveston and Kelly [34] presented a simple yet physically consistent expression for the theoretical number of fibres n_{theo} which are freely orientated in three dimensions crossing a plane of unit area. This

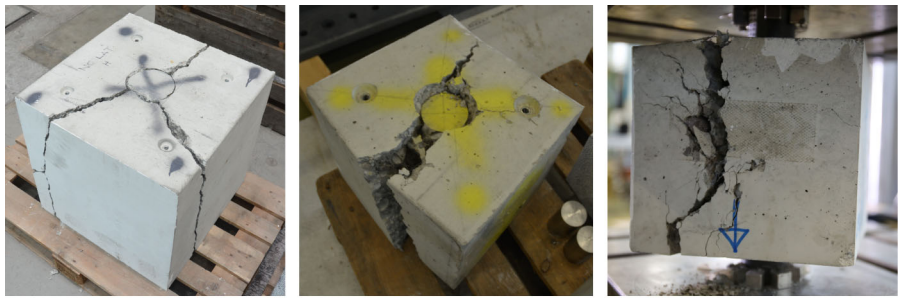

(a) (b) (c)

Fig. 4 Crack pattern of tested double punch samples: **a** F00-600-H; **b** F40-300-H; **c** F80-150-V-cut

Table 3 Measured wedge inclination cot(α) and ratio n_{count} / n_{theo} between counted and theoretical number of fibres crossing the vertical crack where the deformation localised at failure

{fibre dosage} [kg/m3]	{size} [mm]	{loading direction}	cot(α) [−]		n_{count} / n_{theo} [−]	
40 | 80	150	H	2.45	1.81	–	0.77
40 | 80	150	V	2.03	1.97	0.62	1.38
40 | 80	212	H	1.96	2.04	0.58	0.45
40 | 80	212	V	2.30	1.58	0.82	0.87
40 | 80	300	H	2.19	2.27	0.80	0.53
40 | 80	300	V	2.08	2.08	1.18	1.22
40 | 80	424	H	1.96	2.26	0.81	0.69
40 | 80	424	V	2.13	1.60	1.29	1.30
40 | 80	600	H	2.20	2.79	0.50	0.56
40 | 80	600	V	2.49	2.65	0.95	0.96
Mean (CoV)		H	2.08(0.07)	2.23(0.16)	0.67(0.23)	0.60(0.21)
Mean (CoV)		V	2.21(0.09)	1.98(0.22)	0.97(0.28)	1.15(0.19)

expression was derived as $2{\cdot}\rho_f/\left(\pi{\cdot}d_f^2\right)$, where ρ_f is the total volumetric fibre content, and d_f is the diameter of the fibre. To account for boundary and wall effects [35], this expression may be expressed as:

$$n_{theo} = \frac{4 \cdot K_f \cdot \rho_f}{\pi \cdot d_f^2} \tag{3}$$

where K_f is the fibre orientation factor. By assuming that all possible fibre orientations have an equal probability of occurrence, the fibre orientation factor K_f for a fibre in 3D space is $K_f = 1/2$ [36–38]. We note that adopting $K_f = 1/2$ gives the same expression as that derived by Aveston and Kelly. The theoretical number of fibres n_{theo} is therefore 108 and 216 per 100 cm^2 for SFRC unimpeded by boundaries containing 40 and 80 kg/m^3 of fibres used in this study, respectively.

After testing, the number of fibres crossing the localised crack were manually counted to check whether segregation or alignment of the fibres had occurred. For the specimens of larger sizes ($s \geq 300$ mm), the fibres were counted over a cut section approximately parallel to the localised crack. Two areas of 100 cm^2 were randomly selected and inspected at the upper and lower parts of the section. The areas were at least 35 mm (i.e., the length of a fibre) away from the external face of the cube to minimise any biases due to the boundary effects. The number of counted fibres n_{count} between the two areas of the same specimen was similar, meaning that no significant fibre segregation occurred during the casting and compaction operation. The mean value of the two areas is reported in Table 3. The fibre counting in the smaller specimens ($s \leq 212$ mm) was

conducted directly on the localised crack (the specimens were opened across this surface). One area corresponding to half of the crack surface was inspected. The results are shown in Table 3, where the ratio between n_{count} and n_{theo} is presented. The fibres in specimen F40-150-H could not be counted because the specimen was severely damaged after testing when it was force prised opened along the localised crack.

It can be seen that the number of fibres counted for the specimens loaded in V direction was consistently and significantly greater than in the H direction, regardless of the fibre dosage or the size of the specimens. Since all the specimens with 40 or 80 kg/m^3 of steel fibres consisted of the same rheology of SFRC, the difference in the number of fibres relative to the loading direction is attributed to the vibration process during casting. The data clearly indicates that for the mix rheology adopted in this study, the fibres tended to align horizontally with respect to their orientation at casting. Therefore, more fibres bridge vertical cracks (parallel to the casting direction) than horizontal cracks (perpendicular to it), see Fig. 5. The implication of this observation is discussed below. It is worth remarking that some specimens appear to have fewer fibres in both the vertical and horizontal loading directions than the expected theoretical amount. These results are believed to be attributed to the normal variability of the material and the tendency of the crack to localize in sections containing fewer fibres [36–38]. These are important aspects that must be considered in the design of FRC structures.

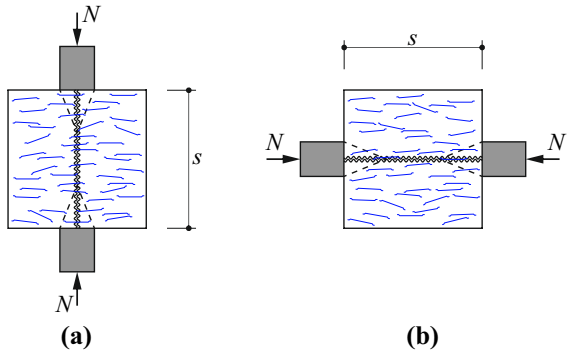

Fig. 5 Schematic drawing of the dominant fibre alignments: **a** Samples with *loading direction* V; **b** samples with *loading direction* H. Note: casting direction = vertical

3.4 Cracking load

Table 4 reports the cracking load, number of radial macrocracks, and number of localised radial cracks at the conclusion of testing for each specimen. For the SFRC specimens, the cracking load is usually clearly identified by a kink in the load (or nominal stress) vs penetration curve (compare Fig. 7). However, for some cubes with 80 kg/m^3 of fibres loaded in the vertical direction, this was not the case. For this reason, the cracking load is unambiguously defined for all specimens as the load at which the average crack width on any cube side attains the threshold value of 0.1 mm.

In line with Chen [20] and Marti [21], a nominal stress is specified in order to compare the different sized double punch tests. The nominal stress is defined the same as in Lee et al. [28] as:

$$\sigma_N = \beta \frac{N}{s^2} \tag{4}$$

where N is the applied load, s represents the side length of the cube, and β is a coefficient whose value, assumed to be constant for geometrically similar structures, is chosen in such a way that σ_N at cracking for a specimen size corresponding to that of the standard cylindrical double-punch test (i.e. s = 150 mm) equals the tensile strength of concrete f_{ct} given by Eq. (1). In this study, a value of $\beta = 0.54$ is adopted for all specimens.

Comparing the cracking loads shown in Fig. 6, it can be concluded that for the SFRC specimens, there is a clear difference in the responses with respect to the loading vs casting directions. For the V specimens, a significantly higher cracking load was seen when compared to the specimens tested in the horizontal direction. Two hypotheses are considered to explain this difference. The first is that some tension is carried by the fibres prior to reaching the crack width threshold set to define the cracking load, with more fibres crossing the cracks in the specimens loaded in the V-direction. The second hypothesis relates to the observed predominant fibre orientation in the horizontal direction due to the casting and vibration procedure, with the fibres being prevalently oriented parallel to the plane where the cracks would form. Considering the interface between the fibres and surrounding matrix to be a weak concrete zone, it is hypothesised that the presence of fibres would locally

Table 4 Cracking load and number of radial cracks of the tested double-punch specimens

{fibre dosage} [kg/m^3]	{size} [mm]	{loading direction}	Cracking load N_{cr} [kN]			Number of cracks	Number of localised cracks
00 | 40 | 80	150	H	125.2	116.6	129.4	2 | 2 | 2	– | 1 | 2
00 | 40 | 80	150	V	131.7	137.6	157.3	3 | 3 | 3	–| 2 | 1
00 | 40 | 80	212	H	268.2	242.9	210.6	3 | 2 | 2	–| 1 | 2
00 | 40 | 80	212	V	260.2	256.3	312.8	2 | 2 | 2	–| 2 | 1
00 | 40 | 80	300	H	470.8	427.3	442.0	3 | 2 | 2	–| 1 | 1
00 | 40 | 80	300	V	460.2	496.1	515.8	3 | 2 | 3	–| 2 | 1
00 | 40 | 80	424	H	863.7	691.5	752.4	3 | 2 | 2	–| 1 | 1
00 | 40 | 80	424	V	865.0	895.9	923.1	3 | 3 | 2	–| 1 | 1
00 | 40 | 80	600	H	1724.2	1347.7	1603.3	3 | 2 | 2	–| 1 | 1
00 | 40 | 80	600	V	1723.4	1779.6	1923.2	3 | 2 | 2	–| 1 | 1

decrease the tensile strength of the concrete along this interface. Consequently, cracks along these interfaces would contain fibres that aren't adequately engaged. Similar observations were made by [40].

Bažant [39] introduced the following nonlinear fracture mechanics-based size-effect relationship for quasi-brittle structures:

$$\overline{\sigma}_{N,cr} = \frac{B_0 \cdot f_{ct}}{\sqrt{1 + \frac{s}{\lambda \cdot D_{max}}}} \tag{5}$$

where $\overline{\sigma}_{N,cr}$ is the prediction for the nominal stress defined in Eq. 1, λ and B_0 are empirical constants, and D_{max} is the maximum aggregate size. As shown by Lee et al. [28], Bažant's size-effect relationship can be fitted to the experimental results to obtain a trend line for the cracking strength for different cube sizes. The obtained trend lines and the corresponding least-square fitting parameters are shown in Fig. 6.

For plain concrete and for the SFRC with fibre dosages of 40 kg/m^3 and 80 kg/m^3, a clear size-effect can be observed in Fig. 6. Nevertheless, based on the obtained data, it cannot be determined whether the fibres enhance or diminish the size effect. The explanatory power of the data is limited because of the relatively small number and limited size range of the test specimens, whereby the capacity of the 5 MN

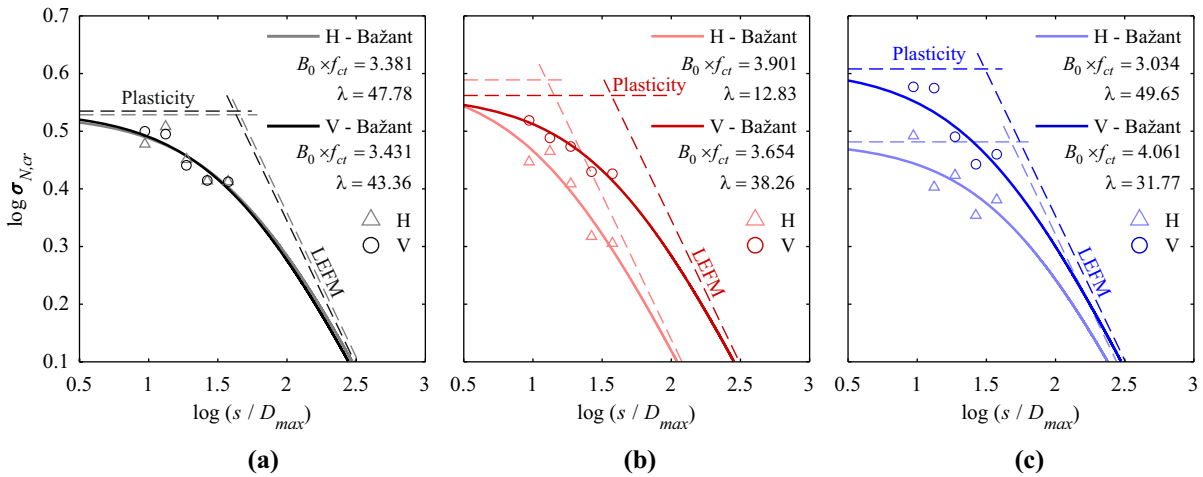

Fig. 6 Log-log plot of the size effect on nominal stress at cracking for **a** plain concrete; **b** fibre dosage of 40 kg/m^3 and **c** fibre dosage of 80 kg/m^3 (the continuous curves denote the fitted size-effect relationship according to Bažant [39], while the dashed lines refer to the solutions of linear elastic fracture mechanics (LEFM) and plasticity)

testing machine governed the maximum specimen size. Therefore, no in-depth analyses and interpretations of size effects are presented here.

3.5 Post-cracking behaviour

Figure 7 presents the post-cracking behaviour of the SFRC specimens. The solid lines represent the nominal stress σ_N plotted against the punch penetration ΔL, and the dashed lines correspond to the *TPCW* plotted with respect to ΔL. The plots on the right side of Fig. 7 compare the tests with the same *fibre dosage*. The curves are shifted horizontally so that the cracking load is attained for a penetration $\Delta L = 0$.

It can be observed that the results are significantly impacted by the presence of the fibres. It can also be seen that the post-cracking strength of the V-specimens is significantly greater than the strength of the H-specimens for all sizes tested. This observation can again be explained by the non-homogenous orientation of the fibres (see Sect. 3.3). Interestingly, it can also be seen that the scatter of the post-peak branches of both the nominal stress and the *TPCW* is quite low for all specimen sizes. This observation indicates a size-independent post-peak response. It is worth noting that the *TPCW* is nearly proportional to the post-cracking punch penetration for all fibre dosages, with a slope that appears to decrease with the fibre dosage. This implies that the less effective the fibres are in transferring tensile forces across cracks, the more the radial cracks will open with a given punch penetration.

4 Crack kinematics

In this section, mechanically consistent expressions are derived to relate the axial displacement of the punch (penetration) to the *TPCW* of cubic double punch specimens. Such expressions are particularly useful to estimate the σ-w relationship (Sect. 5) without the necessity to directly measure the *TPCW*, which greatly simplifies the measurement techniques required during experimentation.

4.1 Existing kinematic models

Consider the response of a SFRC double punch test at the onset of cracking. Once the tangential tensile stress reaches the tensile strength of the concrete matrix, two conical fragments suddenly form below the punches and the surrounding concrete is divided by n radial cracks. Hence, Chen [20] (Fig. 8a) idealised the failure kinematics with rigid body displacements of the two conical fragments (defined by the opening angle α) translating toward each other and laterally displacing the surrounding similarly sized concrete parts.

Fig. 7 Nominal stress and total perimetral crack width (*TPCW*) vs penetration for cast specimens with fibres (the predicted *TPCW* by the kinematics models of Chen [20] and Pujadas et al. [23] are represented on the right plots) ▶

Chen [20] and later Marti [21] idealised the failure mechanism of a cylindrical double punch specimen to consist of (infinitely) many radial cracks. The relative displacement vectors between the conical fragments and the outer concrete segments are inclined at a dilatancy angle ψ to the discontinuity surface. The total punch penetration ΔL is the sum of the penetration of the top and bottom punches, which are theoretically equal. Therefore, according to Chen [20] and Marti [21], a total punch penetration of ΔL corresponds to a lateral displacement of the outer segments of $\tan(\alpha + \psi) \cdot \Delta L/2$, resulting in the sum of all radial crack widths, i.e. a *TPCW,* of

$$TPCW_{Chen} = \pi \cdot \tan(\alpha + \psi) \cdot \Delta L \tag{6}$$

In accordance with plasticity theory and the associated flow rule, Marti [18] assumed the dilatancy angle to be equal to the internal friction angle, $\psi = \varphi = \operatorname{atan}\left(\frac{3}{4}\right) = 36.9°$. On account of the upper-bound theorem of limit analysis, the angle α, which is a free kinematic parameter, must be varied to find the least upper bound solution from limit analysis for the failure load N. For the specimens and punch geometries considered in this study, i.e., $d = h = 4p$, and typical concrete properties used in construction practice, i.e., $f_c / f_{ct} < 15$, the least upper bound is always obtained with an angle $\alpha = \operatorname{atan}(p/h) = 14°$, meaning that the apices of the conical fragments coincide [21].

Following an extensive experimental campaign, Pujadas et al. [23] (Fig. 8b) assumed that a failed specimen contained n major radial cracks that divided the specimen into n segments. For the sake of simplicity, the angle between adjacent crack surfaces

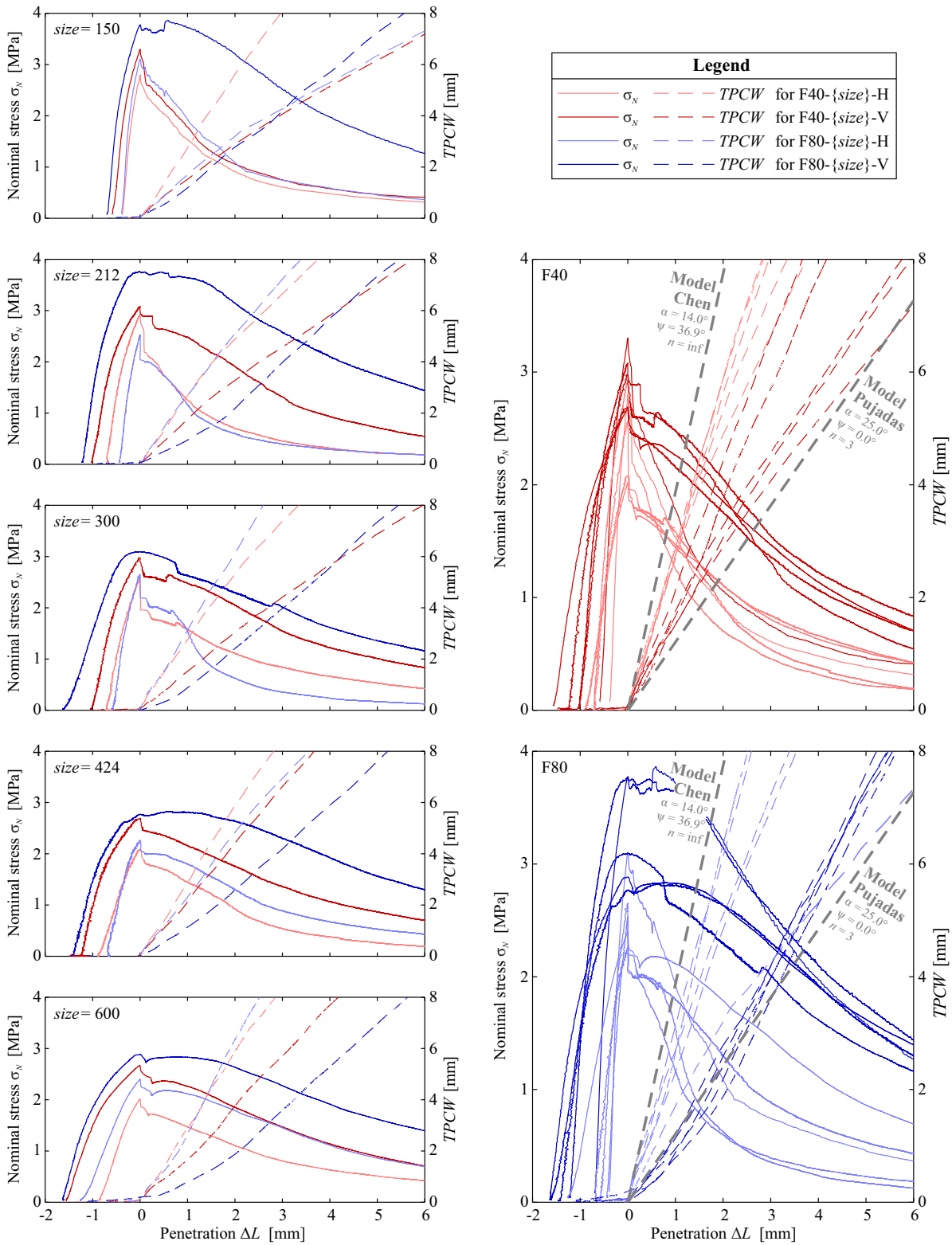
size = 150
size = 212
size = 300
size = 424
size = 600
Nominal stress σ_N [MPa]
TPCW [mm]
Penetration ΔL [mm]
Legend
σ_N TPCW for F40-{size}-H
σ_N TPCW for F40-{size}-V
σ_N TPCW for F80-{size}-H
σ_N TPCW for F80-{size}-V
F40
F80
Model Chen
α = 14.0°
ψ = 36.9°
n = inf
Model Pujadas
α = 25.0°
ψ = 0.0°
n = 3

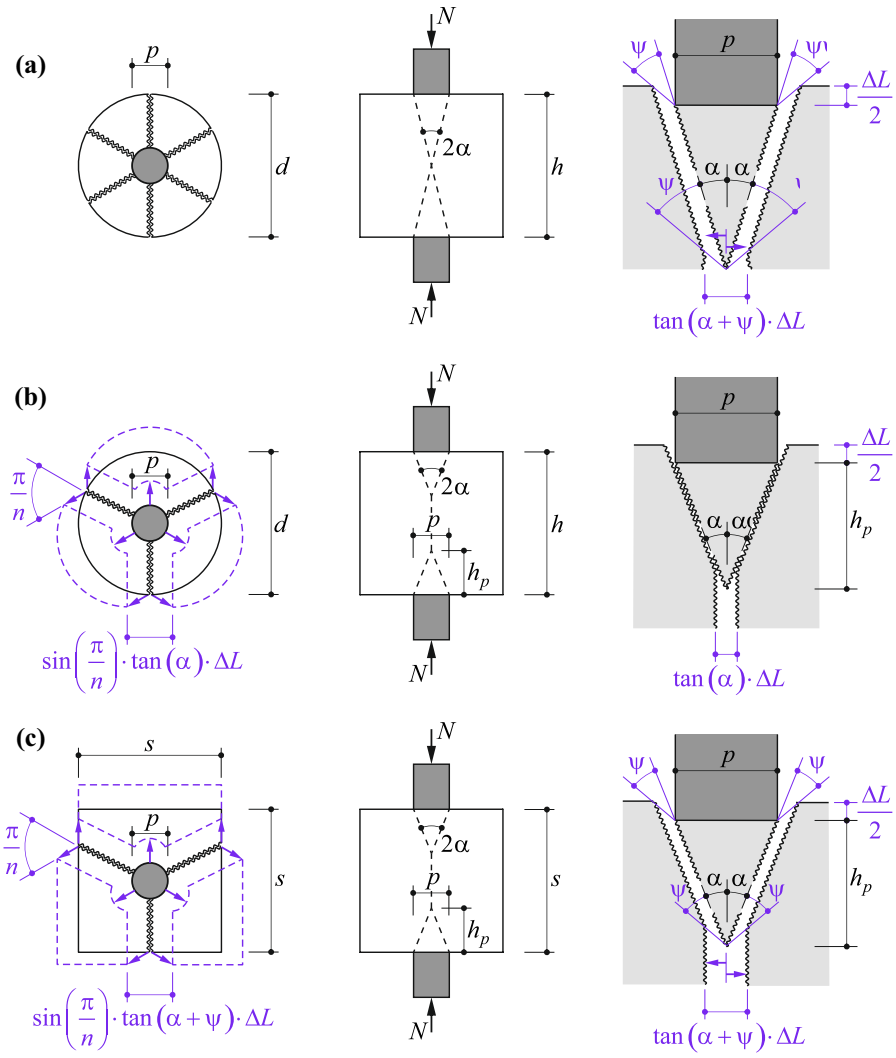

Fig. 8 Kinematic models for double punch tests: **a** Chen (adapted from [21]); **b** Pujadas et al. drawn with three cracks (adapted from [23]); **c** proposed model for cubes assuming three cracks

was assumed to be constant and equal to $2\pi/n$. From the experimental observations, they concluded that a cone angle $\alpha = 25°$ was generally representative for the tested samples. The number of cracks in the experiments was between two and four, but to avoid a biased analysis, the number of cracks was set to $n = 3$. No dilatancy ψ was considered in their model. As such, the *TPCW* was expressed as:

$$TPCW_{Pujadas} = n \cdot \sin\left(\frac{\pi}{n}\right) \cdot \tan(\alpha) \cdot \Delta L \tag{7}$$

The relationships between penetration and *TPCW* predicted by Chen's and Pujadas' models are plotted in Fig. 7 together with the experimental data collected as part of this study. It can be observed that the specimens loaded in the H direction tend to correlate well with Chen's model, whereas the samples loaded in the V direction are better predicted by the model of Pujadas et al. Evidently, neither of these existing models can adequately predict the behaviour of specimens with different fibre dosages and effectiveness.

4.2 Proposed kinematic model

In this study, the two models presented above are combined and applied to a cubic specimen. Accounting for the dilatancy angle ψ and a finite number of cracks n (see Fig. 8c), the following relationship for the *TPCW* is proposed:

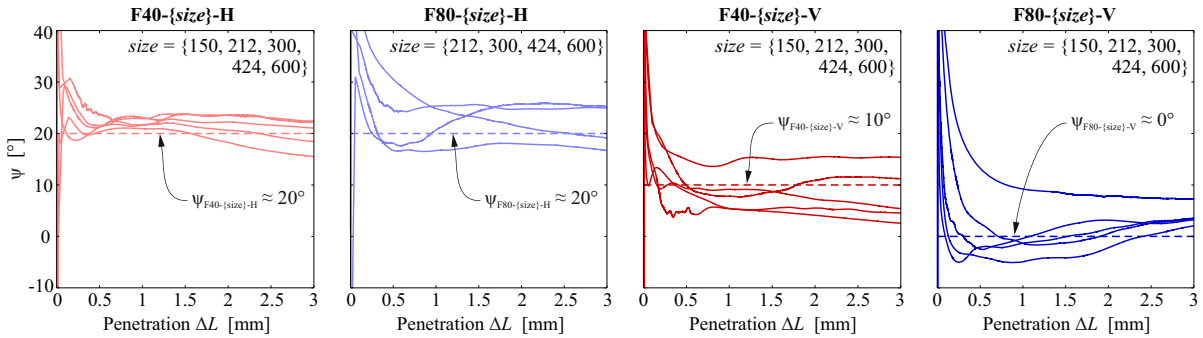

Fig. 9 Estimation of the dilatancy angle ψ for cast specimens with fibres using the proposed kinematic model assuming three cracks

$$TPCW = n \cdot \sin\left(\frac{\pi}{n}\right) \cdot \tan(\alpha + \psi) \cdot \Delta L \tag{8}$$

Based on the experimental observations of this study (see Sect. 3.2), the angle α is set as 25°. Strictly speaking, the assumed mechanism is kinematically not fully consistent. By assuming a finite number of cracks and a perfectly conical wedge, with increasing penetration, the cone slides only on the edges and not the whole surface of its outer counterparts (note that these observations apply to Pujadas' model as well). Nevertheless, considering that in reality the fragments are not perfectly conical but pyramidal, and that the crack surfaces are very rough, the geometric simplifications made are reasonable.

The number of cracks n was found to vary between two and three, with the crack width tending to localize in one or (less frequently) two cracks with increasing punch penetration in the fibre-reinforced specimens (see Table 4). The *TPCW* obtained with Eq. (8) diminished by roughly 23% when $n = 2$ instead of 3 is chosen. To avoid any bias evaluation and fitting to the experimental data, the number of cracks assumed in the model predictions is set for all tests to $n = 3$, with one crack surface passing through the middle of one specimen side (see Fig. 8c). The motivations and implications of this simplification are discussed in Sect. 5.2.

Following the modelling assumptions presented in Sects. 4.1 and 4.2, Eq. (8) can be used to back-calculate the dilatancy angle from the measured *TPCW* and penetration. The obtained values for all SFRC specimens tested in this study are presented in Fig. 9.

The notional dilatancy angles obtained for small penetrations are unreliable due to the uncertainty of the optical measuring systems used to measure the crack widths (particularly for the NDI system, which is ca. 0.1 mm). For penetrations above 0.5 mm, the notional dilatancy angle converged to a constant value. No size effect can be seen for the notional dilatancy angle ψ, however, it is clear that the loading direction and the fibre dosage significantly influenced ψ. For specimens loaded in the horizontal direction, ψ was approximately 20° for both fibre dosages. For those specimens loaded in the vertical direction, ψ was approximately 10° and 0° for 40 kg/m^3 and 80 kg/m^3, respectively. The dilatancy angle of the specimens made of plain concrete could not be determined because the specimens failed too abruptly to perform sufficient crack kinematic measurements. The dilatancy angles of the SFRC specimens are all significantly below the value according to plasticity theory using an associated flow rule of $\psi = \varphi = 36.9°$. Note that the latter value has been verified to be valid and consistent for plain concrete [41, 42].

As the effective fibre content is impacted by the loading direction of the cubes, it may be concluded that the main influential factor pertaining to crack kinematics is the effective fibre content and hence, the effective fibre residual tensile stress. As is seen in Fig. 9, the notional dilatancy angle decreased with increasing effective fibre content. It seems that high effective fibre contents impede the crack opening resulting in lower *TPCW* and consequently yielding a lower notional dilatancy angle according to the modelling assumptions made. A refined quantitative prediction of the dilatancy angle requires further research, related to the dilatancy angle and the effective fibre content / effective fibre residual tensile stress and is beyond the scope of this paper.

However, as a first step in establishing the crack kinematics for this testing configuration, the proposed method allows for the prediction of the *TPCW* based solely on the measured penetration ΔL, noting that the model depends on only a few parameters (i.e., number of cracks n, cone angle α, dilatancy angle ψ) – all of which can easily be determined or estimated with reasonable accuracy. The major benefit of this approach is that it greatly simplifies the measurements required to be gathered during testing. Indeed, following this approach, tracking the cube surfaces with DIC or NDI is no longer necessary.

5 Stress – crack width relationship

The fundamental mechanical property when designing SFRC is its post-cracking residual tensile strength. This can be characterised by means of the direct plots given in Sect. 3.5, as the post-cracking response of a double-punch test is governed by the material's post-cracking tensile response. However, more common and desired for practice are residual tensile fibre stress vs crack width ($\sigma_{t,f}$-w) relationships. In the following, an inverse procedure to obtain such relationships from multidirectional double punch tests is proposed and compared to well-established inverse analysis procedures developed for 3-point bending tests.

5.1 Model for inverse analysis of double punch tests

The inverse analysis model to obtain the $\sigma_{t,f}$-w relationship of SFRC from cubic double punch tests comprises two steps. In the first step, the applied axial load N is related to the residual tensile fibre stress $\sigma_{t,f}$ across the radial cracks. The second step comprises the definition of a reference crack width.

5.1.1 Residual tensile fibre stress $\sigma_{t,f}$

By formulating equilibrium conditions on the failure mechanism described in Sect. 4.2, it is possible to estimate the residual tensile fibre stresses across the radial cracks as a function of the measured axial load. To simplify the calculations, a simple friction model is adopted to describe the interaction of the interface between the cone and the outer concrete segments by considering the symmetry of the specimen. The shear force F_F that acts along the interface between these two elements consists of a frictional component $\mu \cdot F_N$ and a cohesive component $c \cdot A_{cone,n}$, where F_N is the compressive force perpendicular to the surface (as illustrated in Fig. 10), μ is the coefficient of friction, c is the cohesion, and $A_{cone,n}$ is the contact surface area of the outer concrete segments with the corresponding part of the cone:

$$A_{cone,n} = \frac{\pi \cdot s^2}{n \cdot 64 \cdot \sin \alpha} \tag{9}$$

The fibre bridging stress across the conical wedge surfaces are neglected mainly for two reasons: (i) the crack area of the wedge is relatively small compared to the total crack area of the radial cracks; (ii) the low angle of the wedge displacement vector, as illustrated in Fig. 8, leaves most of the fibres ineffective at transmitting stresses across the cracks since the dowel action of the fibres is negligible, short fibres cannot be activated in compression, and fibres oriented close to the crack plane exhibit insufficient anchorage, as described in [35]. As reasoned in Sect. 4.2, strictly geometrically speaking, the cone touches and slides only on the edges of the outer counterpart. However, because of the irregular shape and roughness of the real cone fragments, the assumption of full-surface sliding is justified. Moreover, since the punch penetration is small relative to the cone height, the change in the contact area during sliding is negligible, so it is reasonable to assume $A_{cone,n}$ as constant. Rather than expressing the resultant contact force by its components parallel and perpendicular to the crack, it may be decomposed into its horizontal and vertical components F_X and F_Y, respectively (see Fig. 10b):

$$\begin{cases} F_X = F_N \cdot \cos \alpha - F_F \cdot \sin \alpha \\ F_Y = F_N \cdot \sin \alpha + F_F \cdot \cos \alpha \end{cases} \tag{10}$$

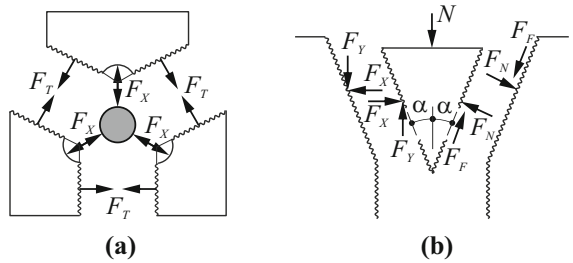

Fig. 10 Equilibrium conditions on the failure mechanism of multi direction double punch tests, particularised for three cracks: **a** plan view; **b** elevation view on the cone

The outer concrete segments are separated by radial cracks opening orthogonally by symmetry, giving rise to tensile fibre bridging forces. The horizontal tensile force between two outer segments is denoted by F_T (see Fig. 10a).

Equilibrium of the conical wedge in the vertical direction gives:

$$N - n \cdot F_Y = 0 \tag{11}$$

Noting that each outer segment is bounded by the upper and lower cone, as well as two adjoining outer segments, equilibrium of horizontal forces yields:

$$2F_T \cdot \sin(\pi/n) - 2F_X = 0 \tag{12}$$

The horizontal tensile force F_T can be then obtained as:

$$F_T = \frac{1}{\sin(\pi/n)} \cdot \left[\frac{\cos\alpha - \mu \cdot \sin\alpha}{\sin\alpha + \mu \cdot \cos\alpha} \cdot \left(\frac{N}{n} - c \cdot A_{cone,n} \cdot \cos\alpha\right) + c \cdot A_{cone,n} \cdot \sin\alpha\right] \tag{13}$$

and the residual tensile fibre stress $\sigma_{t,f}$ is:

$$\sigma_{t,f} = \frac{F_T}{S_c} \tag{14}$$

where S_c is the nominal sectional area of the radial crack surface and can be taken as:

$$S_c = \frac{\kappa \cdot s^2}{2} - \frac{p^2}{4 \cdot \tan\alpha} = s^2\left(\frac{\kappa}{2} - \frac{1}{64 \cdot \tan\alpha}\right) \tag{15}$$

where κ is a coefficient that represents the geometric disparity of the sectional areas of a cube. Generally, the sectional area of each of the radial cracks is different. For $n = 3$ cracks oriented as shown in Fig. 8c, using a value $\kappa = \left(4\sqrt{3} + 3\right)/9 \approx 1.1$ Eq. 15 yields a nominal sectional area corresponding to the average of the three radial sectional areas. A value $\kappa = 1$ would result in a nominal sectional area equal to that of a radial crack perpendicular to the cube edge, i.e., a crack with minimal sectional area.

5.1.2 Reference crack width $\overline{w}$

The choice of a reference crack width to be used in the $\sigma_{t,f}$-w relationship is not obvious, as (i) the number of radial cracks varies, (ii) the cracks rarely open homogeneously along the specimen height, and (iii) the crack width is not uniform among the radial cracks but usually localised in one or two cracks (see Table 4).

In this study, the following definition of the reference crack width is proposed:

$$\overline{w} = \frac{TPCW}{n} \tag{16}$$

with the *TPCW* being the measured total perimetral crack width. In the absence of a direct measurement of *TPCW*, it can be estimated using the kinematic model proposed in Sect. 4.2. This reference crack width $\overline{w}$ is not to be understood as the actual width in the localising crack but as an estimate of the average opening of all cracks. Consequently, the $\sigma_{t,f} - \overline{w}$ relationships obtained with the inverse analysis using the reference crack width $\overline{w}$ should not be interpreted as the 'actual' residual tensile fibre stress for a given crack width. This statement also applies to other testing methods requiring an inverse analysis (e.g., the prism bending test or the round determinate panel test). Even in direct tension tests, the crack often opens unevenly or even partially [11], hindering the definition of an unambiguous crack width. Since the adopted definition of crack width influences the resulting $\sigma_{t,f}$-w relationships, the results of different testing methods might not be always directly comparable. Nevertheless, as long as the reference crack width is clearly defined and applied to all analyses of a given test method, the obtained $\sigma_{t,f}$-w relationships are capable of describing and characterising the post-cracking behaviour of SFRC.

5.2 Results of the inverse analysis of double punch tests

In this section, the model presented in Sect. 5.1. is applied to the experimental results of this study. The residual tensile stress $\sigma_{t,f}$ in each test can be calculated through Eq. (14) with F_T and S_c defined according to Eqs. (13) and (15)), respectively, as shown in Fig. 11. The geometrical parameters s and p are known beforehand. The friction parameters are set to $\mu = 0.75$ and $c = f_c/4$, as typically considered for concrete by the modified Coulomb failure criterion [41]. Based on experimental observations, it is recommended to set the angle of the cone to $\alpha = 25°$, as discussed in Sect. 4.1, and the number of cracks to $n = 3$. While it would be possible to tailor the inverse analysis to the

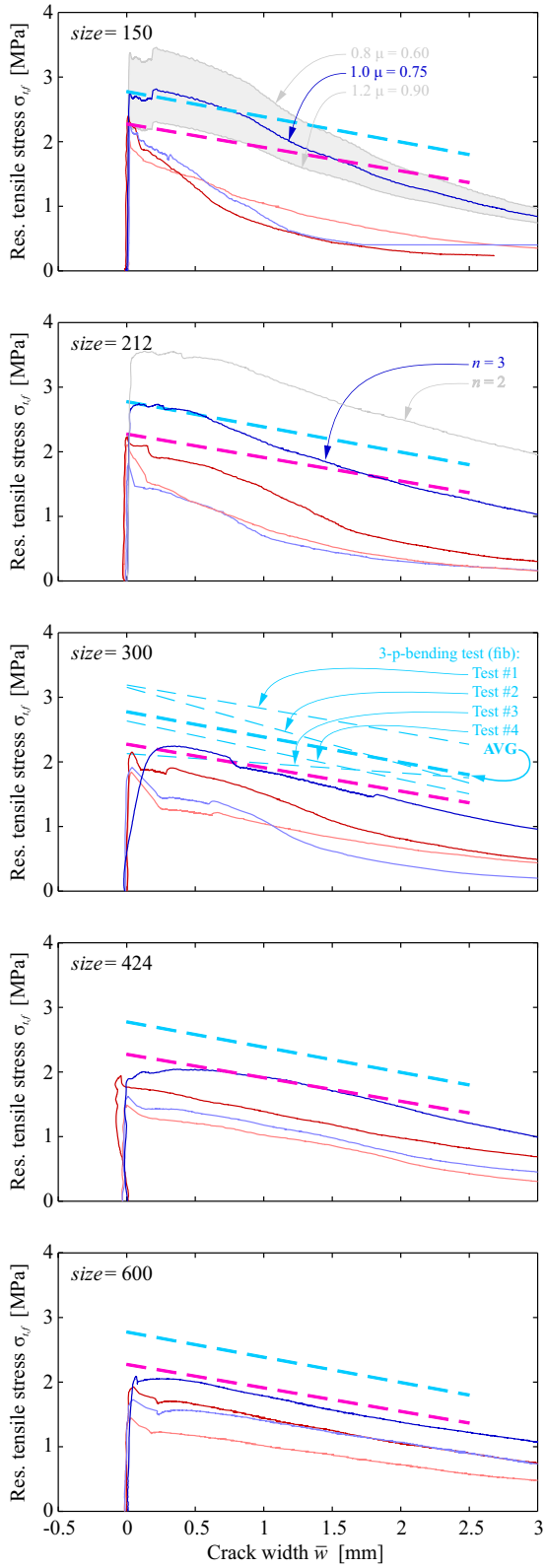
size = 150
0.8 μ = 0.60
1.0 μ = 0.75
1.2 μ = 0.90
size = 212
n = 3
n = 2
size = 300
3-p-bending test (fib):
Test #1
Test #2
Test #3
Test #4
AVG
size = 424
size = 600
Res. tensile stress σt,f [MPa]
Crack width w̄ [mm]

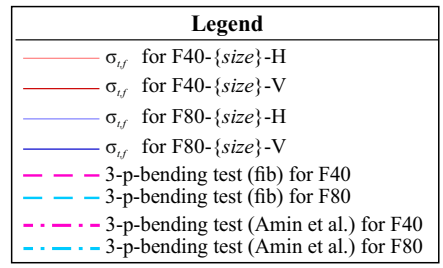
Legend
σt,f for F40-{size}-H
σt,f for F40-{size}-V
σt,f for F80-{size}-H
σt,f for F80-{size}-V
3-p-bending test (fib) for F40
3-p-bending test (fib) for F80
3-p-bending test (Amin et al.) for F40
3-p-bending test (Amin et al.) for F80

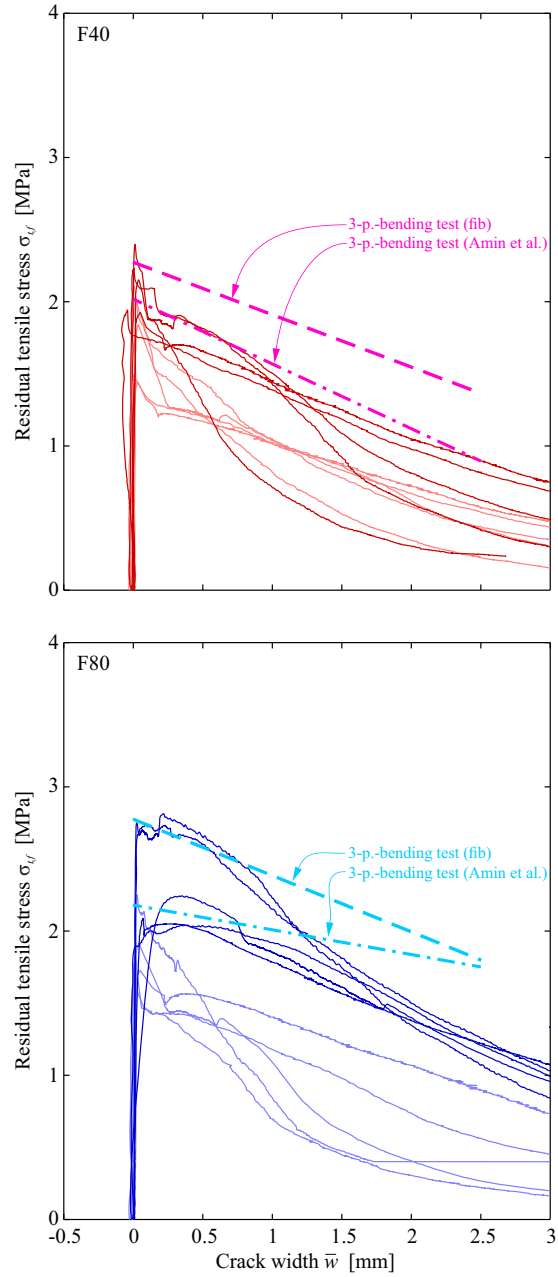
F40
3-p.-bending test (fib)
3-p.-bending test (Amin et al.)
F80
3-p.-bending test (fib)
3-p.-bending test (Amin et al.)
Residual tensile stress σt,f [MPa]
Crack width w̄ [mm]

◀**Fig. 11** Residual tensile capacity of FRC estimated with the proposed inverse analysis of multidirectional double punch tests (computed with n = 3 cracks), including comparison to the results of inverse analyses from 3-point bending tests according to *fib* Model Code 2010 [44] and Amin et al. [8] (the sensitivity of the results to the chosen friction coefficient μ and number of cracks n is shown for specimens of 150 and 212 mm, respectively)

actual failure geometry of each specimen, this would hinder the standardisation of the method and might be prone to biased evaluations. A value of $\kappa = 1.1$ in Eq. (15) should be considered to be consistent with the assumed crack pattern.

An analysis of the sensitivity of the model to the input parameters showed that the results are affected by the chosen value of the friction coefficient μ and the number of cracks n. The influence of a 20% variation in the friction coefficient μ is shown for F80-150-V in Fig. 11. In the same Figure, the influence of the variation in the number of cracks n is presented for F80-212-V. Varying the cohesion c between 0 and $f_c/4$ in Eq. (13) results in a slight variation of the residual tensile stress – equal to approximately 3%. Varying the parameter κ from 1.1 to 1.0 in Eq. (15) has greater significance where an increase in the residual tensile stress of about 11% is achieved.

The general softening trends of the inverse analysis (see Fig. 11) match those observed in the experiments (see Fig. 7). The results of the inverse analysis confirm the finding of Sect. 3.5; there was a clear difference in behaviour between the samples containing 40 and 80 kg/m^3 of steel fibres: higher fibre dosages led to higher residual tensile fibre stresses. The results also indicate a pronounced material anisotropy. The residual tensile fibre stress for the specimens tested in the vertical direction was significantly greater than that of the specimens tested in the horizontal direction. Regarding the size effect, it can be seen from Fig. 11 that the smaller specimens displayed a higher initial residual tensile fibre stress, but exhibited a more pronounced softening response with increasing crack width than the larger specimens. It must be mentioned that the boundary effect could potentially also cause such a behaviour. The boundary effect is characterised by aligned orientation and reduced anchorage strength of fibres located within close vicinity of the formwork, which Stroven and Hu [43] suggested is equal to half the fibre length. The influence of this effect is not within the scope of this paper.

5.3 Comparison between the inverse analysis of double punch tests and 3-point bending tests

In this section, the inverse analysis procedure developed herein for double punch tests is compared to the results of two inverse analysis procedures for 3-point bending tests on notched prisms: the approach contained in the *fib* Model Code 2010 [44] and the procedure proposed by Amin et al. [8]. As described in Sect. 2.1, the samples for the bending and the double punch tests were cast from the same concrete batch and tested approximatively at the same concrete age. The bending inverse analyses are applied to the average results (see Table 2) of four 3-point-bending tests according to EN 14651 [13]. The resulting linear post-cracking constitutive relationships are presented in Fig. 11.

As noted in Sect. 1, although the results from the prism bending tests are widespread and most often used to characterise the behaviour of SFRC at the material level, results from these tests do not yield the "real" σ_f-w relationship. The inverse analysis procedure for indirect tests such as prism bending tests are typically founded on assumptions and simplifications. Indeed, there is still discussion within the scientific community on which inverse analysis method is the most reliable. Hence, results from these tests should not be interpreted as the "correct" σ_f-w relationship and act as the benchmark for the other tests. Furthermore, only one double punch test was carried out for each combination of specimen size, fibre content, and loading direction. This already resulted in a large and demanding experimental campaign. Considering the random nature of the fibre distribution, substantial scatter is expected in the residual tensile response of SFRC samples coming from the same batch – see for instance the σ_f-w relationships obtained from four bending test for *fibre dosage* = F80 in the plot with *size* = 300 in Fig. 11. For these reasons, every conclusion should be made with some caution. Nevertheless, the following observations are noted.

There was a good agreement for the initial residual tensile fibre stress when comparing the results of the bending tests according to *fib* Model Code 2010 and the smaller sized (s = 150, 212 mm) double punch specimens loaded in the V direction (for both fibre

dosages). This is not a surprising observation since both specimens have similar cross-sectional sizes and were tested in the same direction relative to casting. The double punch test on larger cubes with loading direction H led to significantly lower initial residual tensile fibre stresses. An excellent agreement existed between the results of the bending tests according to Amin et al. [8] and the specimens with *fibre dosage* = F40 and *loading direction* = V.

The small double punch test specimens yielded σ_f-w relationships that softened significantly more than the average linear relationship given by the bending tests. The double punch test on larger specimens presented a softening slope similar to that of the bending tests.

Generally, the overall differences between bending tests and double punch tests on similarly sized specimens and loading direction V were relatively small compared to the scatter due to random nature of the fibre distribution. The biggest advantage of double punch test over the bending test is that the double punch test allows an easier investigation of the material anisotropy.

6 Conclusions

The residual or post-cracking tensile response of steel fibre reinforced concrete (SFRC) is typically determined following an inverse analysis of flexural prism tests. However, the anisotropy of the material due to the dispersion and orientation of the fibres cannot be accounted for in these tests. This paper explores the potential and capabilities of multidirectional double punch tests on cubic specimens to analyse anisotropic and size effects when characterising the residual tensile capacity of SFRC. To this end, a new kinematic model based on the previous work of Pujadas [23] and Chen [20] is proposed. The model allows for the prediction of the total perimetral crack width of the cubes based on the measured punch penetration when a direct measurement of the crack width on the four sides of the cube is not available. An inverse analysis procedure was also developed to estimate the σ-w response of SFRC as a function of the applied axial load and the measured (or predicted) total perimetral crack width of the cubes. This inverse analysis is composed of (i) equilibrium relationships between the applied axial load and the tangential stress across the vertical radial cracks and (ii) kinematic modelling relating the total perimetral crack width with the reference crack width, depending on the number of cracks formed in the specimen. To tackle the potential and limitations of this methodology, an experimental investigation was conducted comprising 30 double punch tests on cubes of varying sizes, fibre dosage and loading direction with respect to the casting direction. From the experimental and analytical study conducted, the following conclusions can be drawn:

- The multidirectional double punch tests recorded significantly different residual capacities depending on the loading direction. The post-cracking strength of the specimens loaded in the vertical direction (corresponding to the concrete casting direction) was significantly greater than the strength of the specimens loaded in the horizontal direction for all sizes tested. The examination of the failure surfaces of the tested specimens confirmed that this difference was caused by a biased orientation of the fibres, which tended to align horizontally during the casting procedure.
- A clear size-effect with respect to the cracking load can be observed for plain concrete and SFRC with fibre dosage of 40 kg/m^3 and 80 kg/m^3. However, based on the available data, it is not possible to determine whether adding fibres enhances or mitigates the size effect.
- The angle of the concrete wedges created during the multi-directional double punch tests was approximately 25 degrees, which is in good agreement with previous findings on cylindrical double punch tests. It is recommended to adopt this experimental wedge angle as input for kinematic models used to predict the total perimetral crack width.
- The results of the proposed kinematic model are dependent on the assumed number of cracks and dilatancy angle. Either two or three cracks formed in the tests. The cracks had different openings, with most of the damage localising in a single crack. While the actual number of cracks in the test could be accounted for in the inverse analysis, the preliminary observations of this study suggest that considering three cracks might be simple and effective without significantly affecting accuracy. However, the uncertainty in the number of cracks and the distribution of the total perimetral crack

width is a significant shortcoming of the double punch tests compared to other tests with a unique failure mechanism (e.g., notched three-point bending test).

- The notional dilatancy angle estimated from the experimental results of SFRC cubes using the proposed kinematic model ranged between 0° and 20° depending on the fibre dosage and the loading direction. This value is much smaller than the value derived by plasticity theory with the associated flow rule for plain concrete. Further research is required to clarify the dilatancy angle to be considered depending on the effective fibre content / effective fibre residual tensile stress.
- The results of the proposed inverse analysis method for double punch tests on cubes are generally in-line with the output of well-established inverse analysis methods for three-point bending tests regarding the general post-cracking behaviour of SFRC despite the different modelling assumptions, specimen geometries and effective fibre contents. While the procedure does not yield the "real" residual stress-crack width relationship, the approach gives useful comparative information on the loading direction dependency of the residual tensile stress offered by the fibres. Further investigation is required to prove its reliability as a quantitative tool in general and the appropriate choice of parameters in particular.

Acknowledgements The authors gratefully acknowledge the students Sina Fehr and Vanessa Studer for their valuable support during preparation and testing and Meina Fan for her contribution to the analysis of the experiments.

Funding Open access funding provided by Swiss Federal Institute of Technology Zurich. No other funds, grants, or support was received. The authors have no relevant financial or non-financial interests to disclose. First results from this paper have already been published as a conference paper [28]. It is noted that [28] does not cover the very relevant sections relating to the wedge angle, fibre distribution, crack kinematics and stress—crack width relationship as presented in this paper.

References

1. Shah SP, Rangan BV (1971) Fiber reinforced concrete properties. J Proc 68:126–137. https://doi.org/10.14359/11299
2. Shah SP, Naaman AE (1976) Mechanical properties of glass and steel fiber reinforced mortar. J Proc 73:50–53. https://doi.org/10.14359/11055
3. di Prisco M, Plizzari G, Vandewalle L (2009) Fibre reinforced concrete: new design perspectives. Mater Struct 42:1261–1281. https://doi.org/10.1617/s11527-009-9529-4
4. Hillerborg A (1980) Analysis of fracture by means of the fictitious crack model, particularly for fibre reinforced concrete. Int J Cem Compos 2:177–184
5. van Mier JGM (1996) Fracture processes of concrete. CRC Press, US
6. Van Vliet MRA, Van Mier JGM (1999) Effect of strain gradients on the size effect of concrete in uniaxial tension. Int J Fract 95:195–219. https://doi.org/10.1007/978-94-011-4659-3_11
7. van Mier JGM, van Vliet MRA (2002) Uniaxial tension test for the determination of fracture parameters of concrete: state of the art. Eng Fract Mech 69:235–247. https://doi.org/10.1016/S0013-7944(01)00087-X
8. Amin A, Foster SJ, Muttoni A (2015) Derivation of the σ-*w* relationship for SFRC from prism bending tests. Struct Concr 16:93–105. https://doi.org/10.1002/suco.201400018
9. Rots JG, De Borst R (1989) Analysis of concrete fracture in "direct" tension. Int J Solids Struct 25:1381–1394. https://doi.org/10.1016/0020-7683(89)90107-8
10. Cattaneo S, Rosati G, Banthia N (2009) A simple model to explain the effect of different boundary conditions in direct tensile tests. Constr Build Mater 23:129–137. https://doi.org/10.1016/j.conbuildmat.2008.01.013
11. Amin A, Markić T, Gilbert RI, Kaufmann W (2018) Effect of the boundary conditions on the Australian uniaxial tension test for softening steel fibre reinforced concrete. Constr Build Mater 184:215–228. https://doi.org/10.1016/j.conbuildmat.2018.06.217
12. Mechtcherine V, Schulze J (2006) Testing the behavior of strain hardening cementitious composites in tension, In: G. Fischer, V.C. Li (Eds.), Int. RILEM Workshop High Perform. Fiber Reinf. Cem. Compos. Struct. Appl., RILEM Publications SARL, 2006 https://doi.org/10.1617/2912143942.005
13. EN 14651 (2005) test method for metallic fibre concrete—Measuring the Flexural Tensile Strength (Limit of Proportionality (LOP), Residual), European Committee for Standardization (CEN), Brussels

14. NBN B 15–238 (1992) Test on fibre reinforced concrete - bending test on prismatic samples., Norme Belge, Institut Belge de Normalisation, Brussels
15. C09 Committee ASTM C1018 Test method for flexural toughness and first-crack strength of fiber-reinforced concrete (Using Beam With Third-Point Loading), ASTM International, n.d. https://doi.org/10.1520/C1018-97.
16. Ferrara L, Di Prisco M, Lamperti MGL (2010) Identification of the stress-crack opening behavior of HPFRCC: the role of flow-induced fiber orientation, In: FraMCoS, Jeju, Korea,: pp. 1541–1550.
17. Abrishambaf A, Barros JAO, Cunha VMCF (2013) Relation between fibre distribution and post-cracking behaviour in steel fibre reinforced self-compacting concrete panels. Cem Concr Res 51:57–66. https://doi.org/10.1016/j.cemconres.2013.04.009
18. Mudadu A, Tiberti G, Germano F, Plizzari GA, Morbi A (2018) The effect of fiber orientation on the post-cracking behavior of steel fiber reinforced concrete under bending and uniaxial tensile tests. Cem Concr Compos 93:274–288. https://doi.org/10.1016/j.cemconcomp.2018.07.012
19. Martinelli P, Colombo M, Pujadas P et al (2021) Characterization tests for predicting the mechanical performance of SFRC floors: identification of fibre distribution and orientation effects. Mater Struct. https://doi.org/10.1617/s11527-020-01593-7
20. Chen WF (1970) Double punch test for tensile strength of concrete. ACI J 67:993–995
21. Marti P (1989) Size effect in double-punch tests on concrete cylinders. Mater J 86:597–601
22. Molins C, Aguado A, Saludes S (2009) Double punch test to control the energy dissipation in tension of FRC (Barcelona test). Mater Struct 42:415–425. https://doi.org/10.1617/s11527-008-9391-9
23. Pujadas P, Blanco A, Cavalaro S, de la Fuente A, Aguado A (2013) New analytical model to generalize the barcelona test using axial displacement. J Civ Eng Manag 19:259–271. https://doi.org/10.3846/13923730.2012.756425
24. Pujadas P, Blanco A, Cavalaro SHP, de la Fuente A, Aguado A (2014) Multidirectional double punch test to assess the post-cracking behaviour and fibre orientation of FRC. Constr Build Mater 58:214–224. https://doi.org/10.1016/j.conbuildmat.2014.02.023
25. Monte R, de la Fuente A, de Figueiredo AD, Aguado A (2016) Barcelona Test as an Alternative Method to Control and Design Fiber-Reinforced Concrete Pipes. Struct J 113:1175–1184. https://doi.org/10.14359/51689018
26. Nogueira AB, de Carvalho Ribeiro L, Simão R, Monte RP, de Salvador AD, Figueiredo (2021) Evaluation of the repeatability and reproducibility of the double punch test. Constr Build Mater 268:1211
27. Blanco A, Pujadas P, Cavalaro S, de la Fuente A, Aguado A (2014) Constitutive model for fibre reinforced concrete based on the Barcelona test. Cem Concr Compos 53:327–340. https://doi.org/10.1016/j.cemconcomp.2014.07.017
28. Lee M (2019) Size effect in multiaxial double punch tests on fibre reinforced concrete cubes, in: Proc. 10th Int. Conf. Fract. Mech. Concr. Concr. Struct., IA-FraMCoS, 2019. https://doi.org/10.21012/FC10.234279.
29. Northern Digital Inc., Optotrak Certus HD, Northern Digital Inc., 2014. https://www.ndigital.com/products/legacy-products/.
30. Correlated Solutions, Vic-3D Software Manual, Correlated Solutions Inc., 2019. http://www.correlatedsolutions.com/supportcontent/VIC-3D-8-Manual.pdf.
31. Gehri N, Mata-Falcón J, Kaufmann W (2020) Automated crack detection and measurement based on digital image correlation. Constr Build Mater 256:119383. https://doi.org/10.1016/j.conbuildmat.2020.119383
32. Gehri N, Mata-Falcón J, Kaufmann W (2022) Refined extraction of crack characteristics in Large-scale concrete experiments based on digital image correlation. Eng Struct 251:113486. https://doi.org/10.1016/j.engstruct.2021.113486
33. Fan M (2020) Multiaxial double punch tests on SFRC cubes: Crack kinematics and stress-crack opening relationship, Projet de Fin d'Etudes, École des Ponts - ParisTech / ETH Zürich
34. Aveston J, Kelly A (1973) Theory of multiple fracture of fibrous composites. J Mater Sci 8:352–362
35. Kaufmann W, Amin A, Beck A, Lee M (2019) Shear transfer across cracks in steel fibre reinforced concrete. Eng Struct 186:508–524. https://doi.org/10.1016/j.engstruct.2019.02.027
36. Pfyl T (2003) Tragverhalten von stahlfaserbeton, Doctoral Thesis. ETH Zurich. https://doi.org/10.3929/ethz-a-004502831
37. Deluce JR (2019) Cracking behaviour of steel fibre reinforced concrete containing conventional steel reinforcement, MSc dissertation, University of Toronto, 2011. https://tspace.library.utoronto.ca/handle/1807/29523 (accessed February 15, 2019).
38. Amin A (2015) Post cracking behavior of steel fiber reinforced concrete: from material to structure, Doctoral thesis, School of Civil and Environmental Engineering, The University of New South Wales: Australia
39. Bažant ZP (1999) Size effect on structural strength: a review. Arch Appl Mech 69:703–725. https://doi.org/10.1007/s004190050252
40. Markovic I, Walraven JC, Van Mier JGM (2004) Tensile behaviour of high performance hybrid fibre concrete. In: Proc 5th Inter Conf Fract Mech Conc Conc Struct Fram.-5, Vail, Colorado, USA, 2004: pp. 1113–1120, ISBN: 0-87031-135-2. https://www.ost.ch/de/person/ivan-markovic-1874
41. Marti P (1980) Zur plastischen Berechnung von Stahlbeton. Birkhäuser, Basel, Switzerland
42. Nielsen MP, Hoang LC (2011) Limit analysis and concrete plasticity, 3rd edn. CRC Press, US
43. Stroeven P, Hu J (2006) Effectiveness near boundaries of fibre reinforcement in concrete. Mater Struct 39:1001–1013. https://doi.org/10.1617/s11527-006-9101-4
44. International Federation for Structural Concrete (2013) fib model code for concrete structures 2010. Ernst & Sohn, Berlin